



A mechanism-based framework for the numerical analysis of creep in zircaloy-4

H. Wang^a, Z. Hu^a, W. Lu^a, M.D. Thouless^{a,b,*}

^a Department of Mechanical Engineering, University of Michigan, Ann Arbor, MI 48109, United States

^b Department of Materials Science & Engineering, University of Michigan, Ann Arbor, MI 48105, United States

ARTICLE INFO

Article history:

Received 1 June 2012

Accepted 31 August 2012

Available online 11 September 2012

ABSTRACT

A deformation-mechanism map has been developed for unirradiated zircaloy-4 based on the creep data available from the literature of the last 35 years. These data have been analyzed to identify different creep mechanisms, based on the forms of the relationships between stress, temperature and strain rate. This identification allowed the activation energies and other associated creep parameters to be derived for each mechanism. The creep parameters were used to construct a deformation-mechanism map for zircaloy-4 that shows the conditions under which different mechanisms are dominant. This information provides an important tool for assessing the effects of stress and temperature in design, especially when extrapolating to different regimes. As an example of how this information might be used in a numerical analysis for design purposes, a novel mechanism-based creep framework was implemented within a finite-element code. Although the framework was developed specifically for zircaloy-4, it provides a general example of how mechanism-based creep laws can be implemented into finite-element analyses. This approach allows the creep of complex geometries to be analyzed rigorously, with the dominant deformation mechanisms being identified and evolving automatically in response to the local temperatures and stresses.

© 2012 Elsevier B.V. All rights reserved.

1. Introduction

One of the fundamental challenges of multi-scale modeling in materials science is to develop suitable frameworks that allow the physics of phenomena occurring at the atomistic scale to be incorporated at the continuum scale. As an example, the analysis of creep deformation in large structures of arbitrary shapes may require continuum-level finite-element calculations to compute local stresses and temperatures that need to be integrated with physics-based models of how the local microstructure evolves and how atoms and dislocations move in response to the stresses and temperatures within the evolved microstructure. Owing to the complexities involved, different types of analytical approaches are needed at different scales, and a major challenge involves establishing a framework by which models from different scales can be incorporated at the other scales.

All too often, attempts at multi-scale modeling are focused on the development of models, particularly at the lower length scales, and are stymied when it comes to bridging to larger length scales. Motivated by an ongoing US Department of Energy initiative for multi-scale modeling of nuclear reactors (CASL), we use the example of creep deformation to suggest the sort of framework that could be the basis to incorporate mechanism-based creep models

into finite-element calculations. It should be emphasized that we are not developing creep models but, rather, we are attempting to show one way by which existing atomistic-level creep models might be included in a relatively simple fashion into a commercial finite-element program. The results are limited by the quality of the data available in the literature for creep of zircaloy and UO₂, and the fact that models of microstructure evolution and its effect on creep are not well-developed. In this context, the framework is illustrated primarily by the use of steady-state creep models. However, we will illustrate the form in which lower-level models of the interaction between radiation, temperature, time, microstructure, stress and creep could be framed so that they could be incorporated in a continuum-level creep calculation.

The mechanisms of steady-state creep that are valid when there is no microstructural evolution during creep have been elucidated over the past 60 years, and models for these mechanisms are summarized in Frost and Ashby [9]. The basic mechanisms are diffusional creep in which atoms diffuse in response to a stress gradient between different orientations of grain boundary, dislocation glide in which flow is controlled by the motion of dislocations that may be pinned by microstructural features such as precipitates, and dislocation climb in which thermal energy provides an additional mechanism for dislocations to overcome pinning obstacles. Each of these laws has a characteristic constitutive relationship between stress and strain rate that can be incorporated into finite-element models. Various forms of these constitutive relationships are incorporated into commercial finite-element

* Corresponding author at: Department of Mechanical Engineering, University of Michigan, Ann Arbor, MI 48109, United States.

E-mail address: thouless@umich.edu (M.D. Thouless).

packages such as ABAQUS®. However, the use of single relationships in finite-element codes is only valid within a relatively narrow range of stresses and temperatures, which causes problems for the analysis of large structures in which both of these may vary appreciably.

An alternative approach currently used in finite-element analyses is the use of an empirical equation to describe creep behavior that can incorporate multiple mechanisms and also microstructural changes [28]. In principal, it might be possible to develop a sufficiently inclusive empirical law to accommodate all combinations of stress, temperature and microstructure evolution. However, such an approach suffers from several potential disadvantages stemming from the intrinsic problems of combining many factors into a single monolithic form. In the first place, there are considerable challenges in developing a useful multi-parameter all-inclusive law that embraces all the effects that are of interest. Even an empirical law that forsakes an equation and substitutes in its place a numerical look-up table runs into considerable numerical difficulty when one considers the number of dimensions that such a table would need to have to be useful. However, there are more fundamental concerns with empirical approaches to creep models in that they hide any insight that might be provided by physics, they do not lend themselves easily to a goal of being guided and modified by lower-scale modeling which tends to be done in a mechanistic-specific fashion, and they cannot be used to extrapolate to new design spaces.

In the present work we incorporate the concepts of creep-mechanism maps developed by Ashby and co-workers [9] within a finite-element program. The basic principle behind the construction of creep-mechanism maps is that multiple creep mechanisms operate under a given set of conditions but, generally, one will be rate controlling. By simultaneously evaluating the constitutive equations resulting from mechanistic models for all possible mechanisms that might operate under a given set of conditions, and adding the effects where appropriate, the dominant mechanism emerges automatically from the calculations. No assumptions need to be made about which mechanism might be dominant, and refinement of individual models can be done in isolation from others. Indeed, an initial basic framework can be expanded systematically to include additional models that might be developed as part of an on-going research program. An empirical law or database that convoluted all creep models together would generally have to be re-evaluated if any of the underlying models were to change.

The mechanistic-based models and equations that form the basis of deformation-mechanism maps have been used for 40 years. Their use in a multi-mechanism analysis has been shown for the thermal cycling of metal films [29]. However this analysis was limited to a situation with uniform stresses and temperatures, allowing an analytical approach. There does not appear to have been a systematic effort to incorporate the models into a finite-element code, as part of a multi-scale modeling effort, so that complex 3-D geometries with variable stress and temperatures can be analyzed. This was one of the goals that motivated the present work.

Deformation-mechanism maps can be found in the literature for zirconium, and its alloys [16,27,15]. However, a recent one for zircaloy-4 [15] appears to be incomplete in that it is missing some of the creep mechanisms that are associated with the alloy in the literature. Therefore, the first task of this work was to use data that could be found from the open literature and to interpret them in the context of standard creep mechanisms and develop a more complete deformation mechanism map for zircaloy-4, within the limits of the data and existing models. We then incorporated this map into a commercial finite-element code, and demonstrated its use to analyze some characteristic geometries approximating fuel/clad assemblies in a nuclear reactor. It will be observed from the results we present that the framework automatically allows

dominant creep mechanisms to be identified in different parts of a component, depending on the local stress state and temperature, and also allows these to change as the conditions change.

It is recognized that the creep models we will be using for both materials are incomplete, and are missing a number of important features. A particular limitation is the absence of models linking the evolution of microstructure to temperature, stress, and radiation, and a corresponding link between the resultant microstructure and the creep parameters for different creep mechanisms. Some of these issues will be discussed in this paper with some thoughts on how such models might be designed to interact with a finite-element program within a multi-scale modeling framework. It is hoped that the models and framework presented in this paper will highlight what may be currently missing in the literature and will motivate the development and refinement of suitable mechanistic based-models. It is also noted that, we have not yet included the deviatoric and volumetric strains that can be induced by radiation effects alone into the framework. This is a project that is currently in progress.

2. Development of a multi-mechanism creep model for zircaloy-4

A multiple-mechanism description of creep relies on the development of distinct constitutive equations from mechanism-based models for each individual mechanism that acts in a material [9]. These equations are cast as a relationship between the effective shear-strain rate, $\dot{\gamma}$, and the effective shear stress, $\bar{\tau}$, which are related to the principal normal strains and stresses by

$$\dot{\gamma} = \left\{ \frac{2}{3} [(\dot{\epsilon}_1 - \dot{\epsilon}_2)^2 + (\dot{\epsilon}_2 - \dot{\epsilon}_3)^2 + (\dot{\epsilon}_3 - \dot{\epsilon}_1)^2] \right\}^{1/2} \quad (1a)$$

$$\bar{\tau} = \left\{ \frac{1}{6} [(\sigma_1 - \sigma_2)^2 + (\sigma_2 - \sigma_3)^2 + (\sigma_3 - \sigma_1)^2] \right\}^{1/2}. \quad (1b)$$

The use of an effective stress to describe creep is predicated on an assumption of isotropy. While many zircaloy-4 components exhibit texture in their grain structures, the consistency of the creep data in the literature indicated that texture does not provide a significant effect on creep, so an assumption of isotropy is valid when considering only the effects of stress on creep. It is recognized that texture effects need to be included in any discussion of radiation growth and creep.

With the exception of dislocation glide, the individual constitutive equations that are derived from the lower-level models will generally be of the form

$$\dot{\gamma}_n = A_n f_n(\bar{\tau}) \exp(-Q_n/RT), \quad (2)$$

for a constant microstructure, and where the subscript n indicates a particular mechanism. In this expression, Q_n is the activation energy of the mechanism for the material in question, T is the absolute temperature, R is the molar gas constant, f_n is the functional dependence of strain rate on stress for the mechanism as it operates in the material, and A_n is a material parameter that depends on the mechanism and microstructure. Unless any are mutually exclusive, the mechanisms are assumed to operate simultaneously within a numerical model under all conditions. Generally, owing to the different activation energies and stress dependencies, one mechanism automatically dominates under a given set of conditions. However, this dominant mechanism evolves naturally without any external selection, and automatically changes as the conditions change. This automatic identification of the dominant mechanism is a very powerful advantage of using a multi-mechanism analysis for numerical purposes.

The microstructural parameters, A_n , will generally evolve with time during service, and will depend on the integrated history of time, temperature, stress and radiation. In a fully-established multi-scale framework, the continuum finite-element calculations that include the creep models would probably be separated from any calculations of microstructure evolution, since they would employ different numerical approaches. The finite-element calculations with the creep models would give information on the temporal evolution of temperature, stress and deformation for each element. These parameters would then be the inputs to microstructure calculations, along with information on the radiation flux and chemical environment, to produce modified values for the microstructural parameters that could be returned to the finite-element model to calculate the creep rates in subsequent increments of time. Currently, the models and data for microstructural evolution and its effects on creep parameters are not sufficient to be useful. Therefore, we assume representative steady-state microstructures and creep rates in our simulations. However, we will illustrate the principles of how one might incorporate microstructure evolution in the framework, using a simple empirical model for work hardening with dislocation glide.

2.1. Creep mechanisms for zircaloy-4

Based on the data and models available in the literature, the multi-mechanism model for zircaloy-4 was predicated on four major creep mechanisms: (i) diffusional creep, (ii) power-law creep, (iii) breakdown of power-law creep, and (iv) dislocation glide. Standard models for these mechanisms [9] have been used, and values for the appropriate parameters for zircaloy-4 have been deduced from a variety of different sources, as described in the sections that follow. At this juncture, the models only include the effects of stress and temperature. Incorporating the effects of radiation (as it relates to microstructural evolution, and the evolution of volumetric and deviatoric strain), and its interaction with a time-dependent 3-D stress state is the subject of an on-going project.

2.1.1. Dislocation glide

At very high stress levels, deformation is dominated by dislocation glide. This is the dominant mechanism associated with yield, and is controlled by the ability of dislocations to move along glide planes under the influence of a shear stress. The general form of the creep equation for this mechanism is [9]

$$\dot{\gamma}_g = \dot{\gamma}_0 \exp \left[-\frac{Q_g}{RT} \left(1 - \frac{\bar{\tau}}{\tau_g} \right) \right], \quad (3)$$

where $\dot{\gamma}_0$ is a normalizing constant, Q_g is the activation energy for dislocation glide, and τ_g is the shear strength required to overcome the barriers to dislocation glide at 0 K. This equation can be rearranged as

$$\bar{\tau} = \tau_g + T \frac{R\tau_g}{Q_g} \ln \left(\frac{\dot{\gamma}_g}{\dot{\gamma}_0} \right), \quad (4)$$

to provide a very distinctive signature for dislocation glide, as opposed to any other creep mechanism, by plotting the stress required to maintain a fixed strain rate as a function of temperature. Such a plot is linear decay with temperature for glide (since $\dot{\gamma}_g < \dot{\gamma}_0$), as opposed to the exponential inverse temperature decay generally valid for creep.

A paper by Derep et al. [5] provides data for the creep of zircaloy-4 that appear to be in the regime of dislocation glide. These data form the basis for deducing the creep parameters of Eq. (4). Fig. 1 shows a plot of the data for an effective plastic strain of 3.5% expressed in terms of the temperature-dependent yield strength as described by Eq. (3). Extrapolation of the data to 0 K, allows the 0 K yield

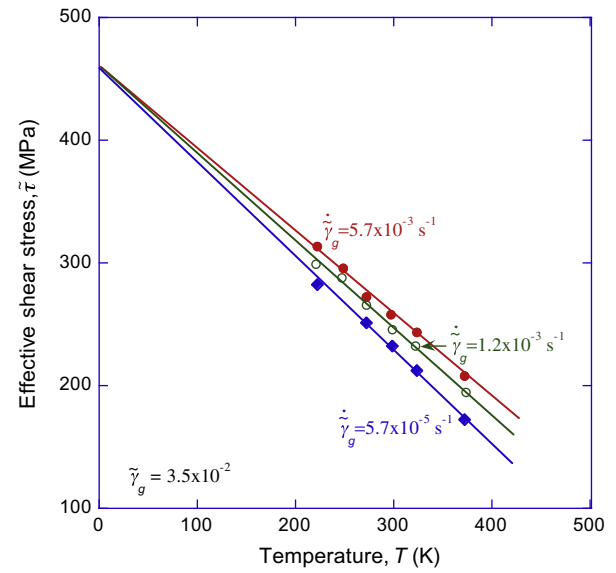


Fig. 1. Data re-plotted from Derep et al. [5] showing the temperature dependence of the shear strength at different strain rates and at an effective strain of 3.5%. From this plot an effective shear strength at 0 K of 460 ± 10 MPa can be deduced. Similar calculations for other extents of plastic strain can also be done using the data of Derep et al. [5].

strength, τ_g , to be deduced as 460 ± 10 MPa. In Fig. 2, the data are re-expressed as an Arrhenius plot in the form suggested by Eq. (3). From this plot, it can be seen that the activation energy for dislocation glide, Q_g , is 175 ± 5 kJ/mol: a value that is very consistent with the activation energy for glide in zirconium quoted by Sargent and Ashby [27]. Finally, Fig. 3 shows a fit to the data, using the uncertainty in Q_g , allowing the value of the normalizing constant, $\dot{\gamma}_0$, to be determined as 10^{11} /s. The equation for creep from dislocation glide for zircaloy-4 with 3.5% plastic strain is therefore given by

$$\dot{\gamma}_g = 10^{11} \exp \left[-\frac{175 \pm 5 \times 10^3}{RT} \left(1 - \frac{\bar{\tau}}{460} \right) \right] /s, \quad (5)$$

where $\bar{\tau}$ is in MPa.

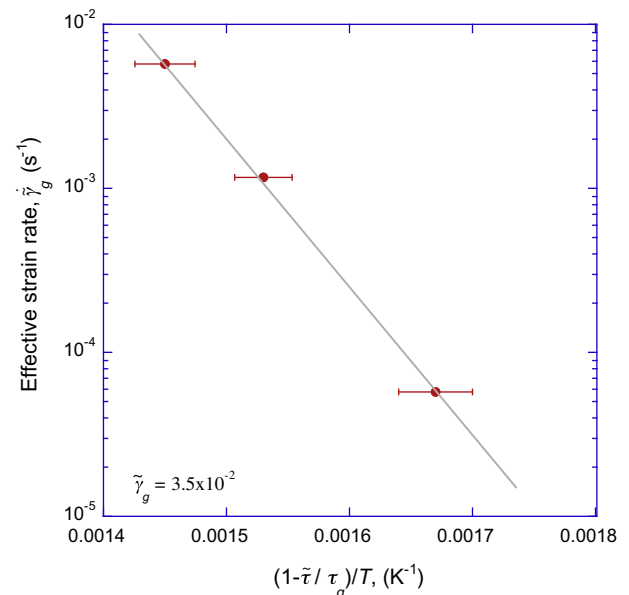


Fig. 2. Data re-plotted from Derep et al. [5] showing the temperature dependence of the strain rate at an effective strain of 3.5%. From this plot an activation energy of 175 ± 5 kJ/mol can be found.

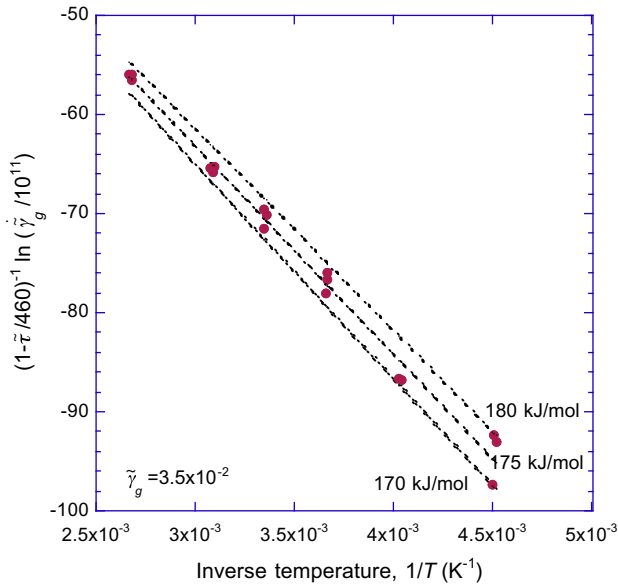


Fig. 3. Data from Derep et al. [5] re-plotted in the form of Eq. (4) to show the normalizing constant for dislocation glide in this system can be taken to be $10^{11}/s$.

The work-hardening curves of Derep et al. [5] also allow the effect of plastic strain, $\dot{\gamma}_g$, on the 0 K shear strength τ_g to be determined as

$$\tau_g = 540 \dot{\gamma}_g^{0.06} \quad (6)$$

above a value of 370 MPa for annealed zircaloy-4. Further examination of the data in Derep et al. [5] verified that the activation energy and form of Eq. (5) are consistent with the data for different levels of plastic strain. Therefore, this equation was used in the numerical modeling, with τ_g being taken as a function of the plastic strain. In particular, the creep rate for dislocation glide in *annealed* zircaloy-4 was taken to be

$$\dot{\gamma}_g = 10^{11} \exp \left[-\frac{175 \pm 5 \times 10^3}{RT} \left(1 - \frac{\tilde{\tau}}{370} \right) \right], \quad (7)$$

with the value of τ_g changing from 370 MPa for strain-hardened materials (Eq. (6)).

2.1.2. Power-law creep and power-law breakdown

In the dislocation-glide regime of deformation, dislocations cut or bow their way past obstacles. However, thermal energy provides an alternative mechanism for dislocations to get around obstacles by climbing out of the glide plane, enabled by diffusion of atoms along the core of the dislocation or away from the core through the lattice. These mechanisms of dislocation climb are responsible for the deformation regime known as power-law creep, in which there is a power-law relationship between the strain rate and stress. However, modeling of this regime is complicated by the fact that there is a broad transition to dislocation glide associated with an apparent increase in the power-law exponent. A general expression that captures both power-law creep and the transition, known as power-law breakdown, is given by [9]

$$\dot{\gamma}_p = \frac{A_p G}{T} \left[\sinh h \left(\frac{\beta \tilde{\tau}}{G} \right) \right]^n \exp \left(-\frac{Q_p}{RT} \right), \quad (8)$$

where G is the shear modulus of the material, Q_p is the activation energy for dislocation climb by diffusion through the lattice,¹ A_p

¹ In many materials, Q_p is equal to the activation energy for lattice diffusion, Q_L . However, Zr alloys appear to exhibit an anomaly in this regard, with Q_p being much larger than Q_L [9,27].

and β are material constants, and n is the power-law-creep exponent. In this work, it was assumed that the shear modulus of zircaloy-4 is given by [28]:

$$G = 39400 - 13.4T \text{ MPa}. \quad (9)$$

For relatively low stresses, $\tilde{\tau} < 0.8G/\beta$, Eq. (8) reduces to the classical form of equation for power-law creep [9]:

$$\dot{\gamma}_p = (\beta^n A_p) \frac{G}{T} \left(\frac{\tilde{\tau}}{G} \right)^n \exp \left(-\frac{Q_p}{RT} \right). \quad (10)$$

At higher values of stress, Eq. (8) reduces to the power-law breakdown form of [9]

$$\dot{\gamma}_p = \left(\frac{A_p}{2^n} \right) \frac{G}{T} \exp \left(\frac{\beta n \tilde{\tau}}{G} \right) \exp \left(-\frac{Q_p}{RT} \right) \quad (11)$$

In the section that follows, the material parameters β , n and A_p for zircaloy-4 are determined from data collected from the many sources in the literature that have appeared over the past 35 years.

Inspection of the literature indicated that the data could be divided into two groups, those that appeared to be described by the power-law creep of Eq. (10), and those that appeared to be described by the power-law break-down of Eq. (11). These two groups of data were analyzed separately to determine the creep parameters and, as will be seen, there is good consistency between the two sets of data, indicating that Eq. (8) is a good description of the creep behavior in this regime. In the analysis that follows, all the quoted stresses and strain rates have been converted to effective stresses and strains, so that both multiaxial and uniaxial data could be used. Again, the consistency between all the sets of data indicates the validity of assuming isotropy and the use of effective stress and strain to describe creep. Fig. 4 presents creep data [3,6,10,15,20,31] over the temperature range of 727–1073 K and at values of effective shear stress in the range of about $10^{-4}G$ to about $2 \times 10^{-3}G$. The log–log plot of Fig. 4 indicates an average power-law exponent of $n = 5.1 \pm 0.5$ for all the reported data. The

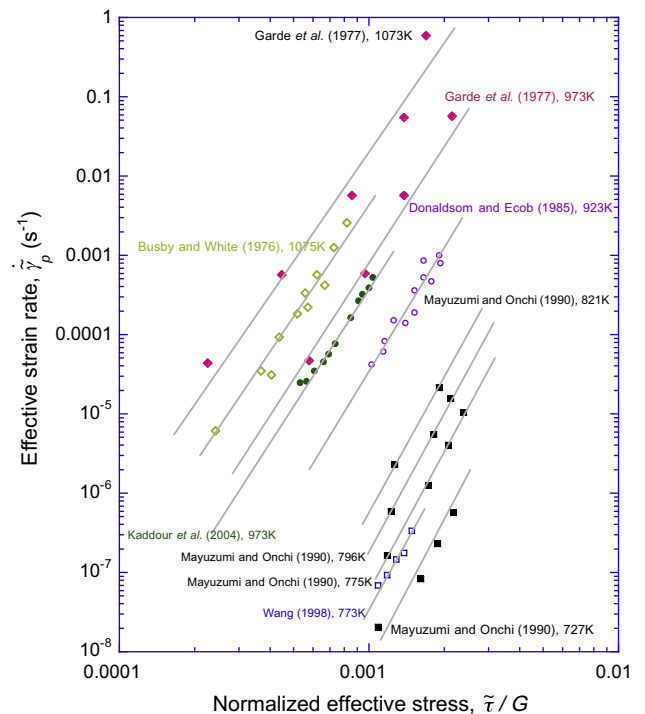


Fig. 4. Data reproduced from a number of sources [3,6,10,15,20,31] showing that the value for the power-law creep exponent, n , is 5.1 ± 0.5 .

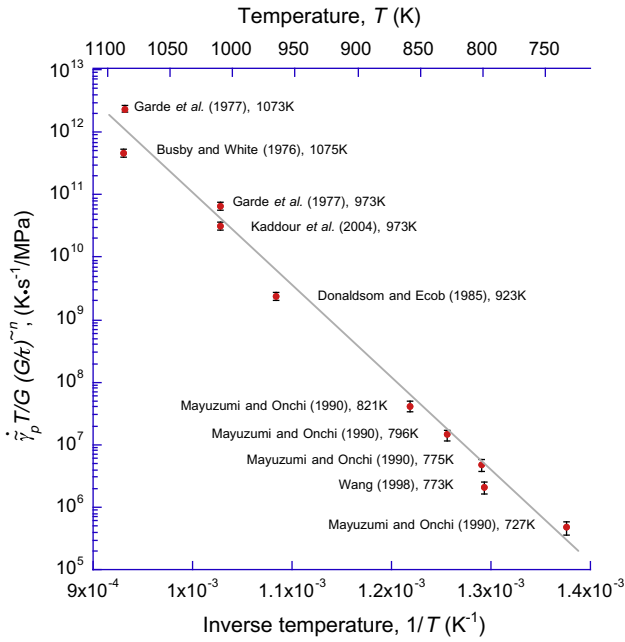


Fig. 5. The data from Fig. 4 re-drawn to show that the activation energy for power-law creep is 285 ± 20 kJ/mol.

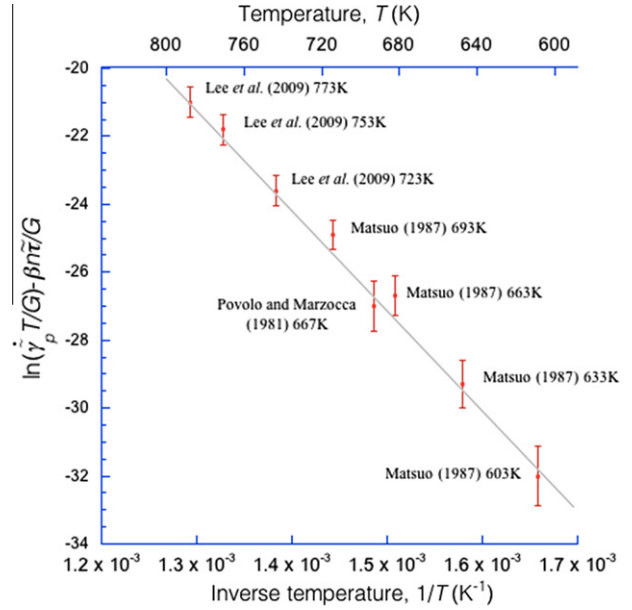


Fig. 7. Data re-plotted from Fig. 6, indicating an activation energy of about 265 ± 20 kJ/mol, consistent with the activation energy deduced from Fig. 5.

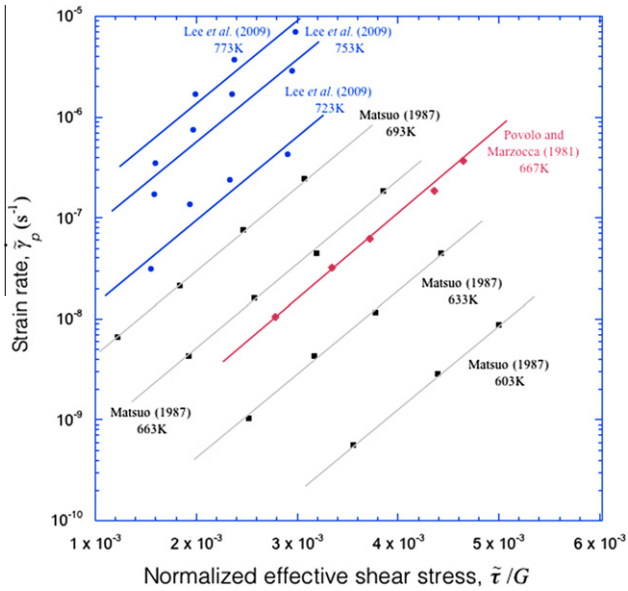


Fig. 6. Creep data [18,19,24] that appear to be in the regime of power-law breakdown, indicating that the value of the constant βn is 1900 ± 200 .

activation energy could then be found by re-plotting the data from Eq. (10) in the form

$$\ln \left[\frac{\dot{\gamma}_p T}{G} \left(\frac{G}{\bar{\tau}} \right)^n \right] = -\frac{Q_p}{RT} + \ln(\beta^n A_p), \quad (12)$$

as shown in Fig. 5. This somewhat complicated form of an Arrhenius plot was chosen because it permits all the data from Fig. 4 to be plotted simultaneously, and the error bars include the uncertainty associated with the value of the power-law exponent. All the data combine to indicate an activation energy of 285 ± 20 kJ/mol. The plot also allows the creep constant $\beta^n A_p$ to be determined. However, the value of this constant depends on n , and cannot be determined

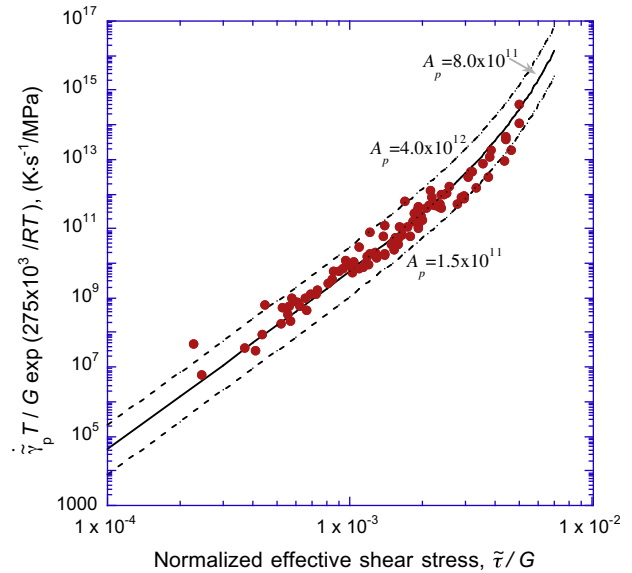


Fig. 8. A comparison between the sinh law of Eq. (14) and all the creep data assembled in Figs. 4 and 6.

independently. For example, if n is taken to be 5.1, then $\beta^n A_p = 6 \times 10^{25}$ K/MP s with upper and lower bounds of 15×10^{25} and 2×10^{25} K/MP s, respectively

Fig. 6 presents creep data from the literature [18,19,24] in a slightly lower temperature range (603–733 K), but in a higher effective shear stress range ($2 \times 10^{-3}G$ – $5 \times 10^{-3}G$). These data are presented on a log-linear plot, showing the linearity that is expected for the power-law-breakdown regime. The slopes of all these different sets of data give an essentially constant value of βn of 1900 ± 200 . It should be noted that the individual data sets also give reasonably linear plots on a log–log plot, but with slopes that systematically change with temperature. The temperature-independent slopes of Fig. 6 indicate that the data are better described by power-law breakdown. The activation energy for

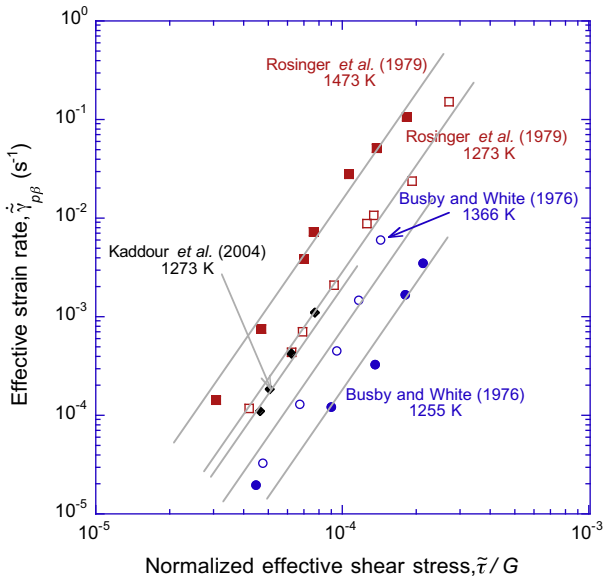


Fig. 9. Data reproduced from a number of sources [3,15,33] showing the value of the power-law creep exponent is 4.0 ± 0.6 for the β phase of zircaloy-4.

power-law breakdown can be deduced in a similar fashion to how the activation energy was determined for the power-law creep regime. Eq. (11) can be re-expressed as

$$\ln\left(\frac{\dot{\gamma}_p T}{G}\right) - \left(\frac{\beta n \tilde{\tau}}{G}\right) = -\frac{Q_p}{RT} + \ln\left(\frac{A_p}{2^n}\right), \quad (13)$$

and is plotted in Fig. 7. As with Fig. 5, the uncertainties of the data and the parameter βn are represented in the error bars of the plot. The slope of the best-fit line gives an activation energy of 265 ± 20 kJ/mol, which is consistent with the activation energy calculated from the previous set of data. The value of A_p that is calculated from the intercept of Fig. 7 is dependent on the choice of βn . If this parameter is taken to be 1900, and n is taken to be 5.1 (so that

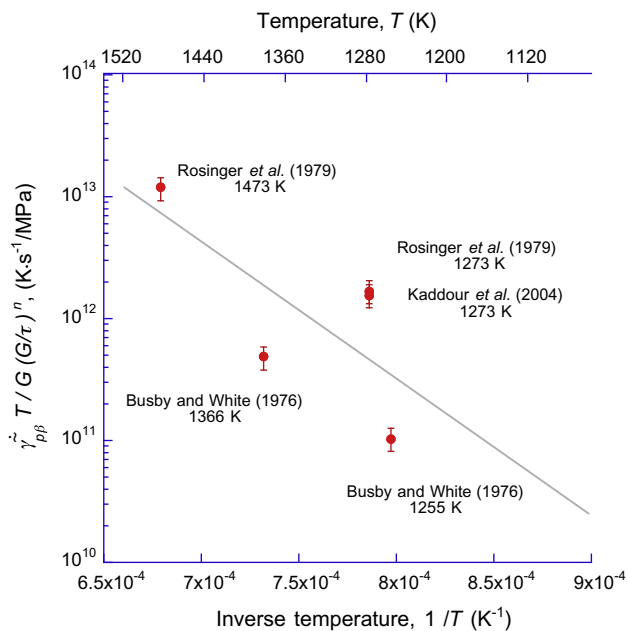


Fig. 10. The data from Fig. 9 re-drawn to show that the activation energy for power-law creep in the β phase is 220 ± 60 kJ/mol.

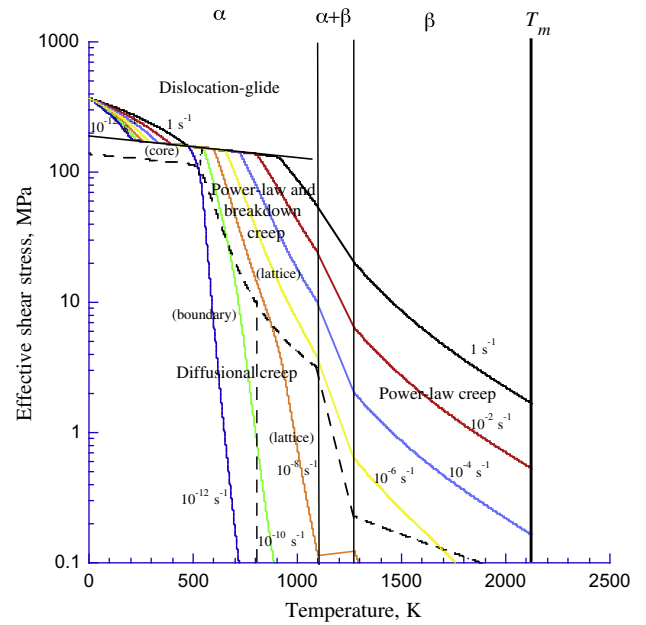


Fig. 11. A deformation-mechanism map drawn using the equations presented in Section 2 of this paper for unirradiated zircaloy-4 with a grain size of $150 \mu\text{m}$.

$\beta = 370$), then $A_p \approx 4 \times 10^{12}$ K/MP s, ranging from between 4×10^{12} K/MP s and 1.5×10^{11} K/MP s. This is very consistent with the value of 5×10^{12} K/MP s calculated in the previous paragraph for $n = 5.1$ and $\beta = 370$.

In conclusion, the two sets of data from the literature which fall into either the power-law or power-law break-down regime show a remarkable consistency in the creep parameters, suggesting that both regimes can be reasonably described by a single sinh law of the form:

$$\dot{\gamma}_p = \frac{8 \times 10^{11} G}{T} \left[\sinh\left(\frac{370 \tilde{\tau}}{G}\right) \right]^{5.1} \exp\left(-\frac{275 \times 10^3}{RT}\right) \quad (14)$$

As shown in Fig. 8, the full range of the uncertainty in the model can be captured by putting a relatively small uncertainty on the scaling parameter, A_p , with it varying between about 4×10^{12} and 1.5×10^{11} K/MP s.

In general, it is expected that power-law creep will be controlled by core diffusion at lower temperatures. However, an extensive search of the literature did not reveal creep data for zircaloy-4 below about 600 K; all the power-law creep data above this temperature are consistent with a single mechanism of lattice-controlled climb. Therefore, it appears that any transition between lattice-controlled and core-controlled power-law creep is below 600 K, and the parameters for core-controlled power-law creep specific to zircaloy-4 are not currently available. In the absence of better data, and to provide a place-holder for this mechanism we have adapted a value for the activation energy of core-diffusion in zirconium of $Q_c = 125$ kJ/mol from Sargent and Ashby [27]. This would appear to be justified because the activation energy for lattice-controlled power-law obtained in the present work for zircaloy-4 is essentially identical to the value quoted by Sargent and Ashby for zirconium (275 kJ/mol versus 270 kJ/mol). A value for the scaling parameter was then chosen arbitrarily to provide a match between the two regimes of power-law creep, with an assumed transition between lattice and core-controlled power-law creep at 550 K at a strain rate of 10^{-9} s^{-1} . This results in an equation for core-diffusion controlled creep of

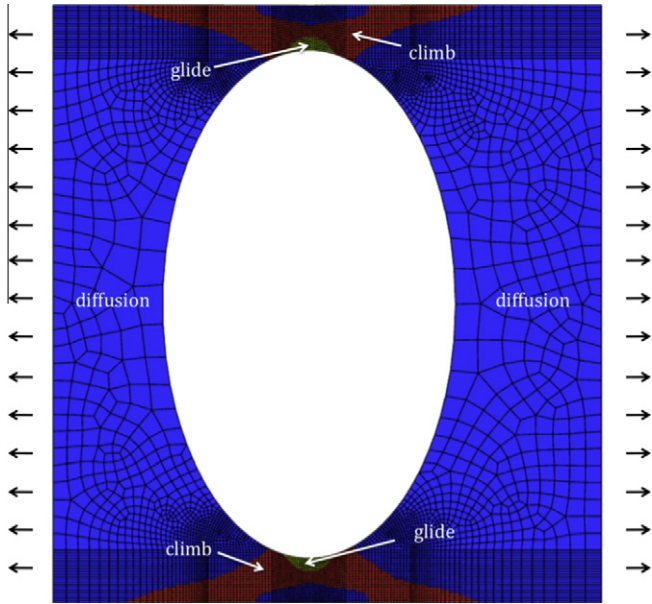


Fig. 12. The dominant relaxation mechanisms operating at 600 K after 1 s with a strain applied at a uniform rate of $2.5 \times 10^{-3}/s$ to the ends of a square sheet of zircaloy-4 containing an elliptical hole.

$$\dot{\gamma}_c = 100 \frac{G}{T} \left(\frac{\sigma_s}{G} \right)^2 \left[\sinh \left(\frac{370\sigma_s}{G} \right) \right]^{5.1} \exp \left(-\frac{125000}{RT} \right) /s. \quad (15)$$

However, it is emphasized that we have not found any experimental data in the literature in a suitable range of stresses and temperatures to validate these parameters for core-diffusion controlled creep.

2.1.3. Diffusional creep

Diffusional creep is associated with the diffusion of atoms driven by gradients in the normal stresses along grain boundaries, and is identified by strain rates that are linear with stress. It generally dominates over other creep mechanisms at low stresses. Diffusional creep, which includes effects of grain-boundary sliding [26] can be characterized by two mechanisms of diffusion: lattice diffusion [21,13] and grain-boundary diffusion [4]. While both mechanisms exhibit the same linear dependence on stress, each has a different dependence on temperature and grain size. *Nabarro-Herring*, or *lattice-controlled*, creep is described by an equation of the form

$$\dot{\gamma}_l = \frac{A_l}{Td^2} \bar{\tau} \exp \left(-\frac{Q_l}{RT} \right) \quad (16a)$$

where d is the grain size, and Q_l is the activation energy for diffusion through the lattice. *Coble*, or *boundary-controlled*, creep is described by an equation of the form

$$\dot{\gamma}_b = \frac{A_b}{Td^3} \bar{\tau} \exp \left(-\frac{Q_b}{RT} \right) \quad (16b)$$

where Q_b is the activation energy for diffusion along grain boundaries.

A number of authors have reported linear creep in zircaloy-4 at relatively low stresses [30,31,15], and other forms of zirconium [2,22,7,25,11,12]. Unfortunately, these data are not sufficiently complete in terms of grain-size and temperature dependence to be useful in deducing the relevant creep parameters. Therefore, in the absence of more appropriate experimental data, we have assumed that the diffusional creep parameters of zircaloy-4 can be

described by the parameters given by Sargent and Ashby [27] for α -zirconium:

$$Q_l = 190 \text{ kJ/mol}, \quad A_l = 2.1 \times 10^{-3} \text{ K m}^2/\text{MPa s},$$

$$\text{and } Q_b = 120 \text{ kJ/mol}; \quad A_b = 1.8 \times 10^{-11} \text{ K m}^3/\text{MPa s}.$$

2.1.4. Phase transitions

There is a phase transition in zircaloy-4 that begins to take place at about 1100 K, when the α phase of zirconium transforms to the β phase. This transition is complete at around 1200 K. There are some data in the literature for the creep of zircaloy-4 at these higher temperatures in the power-law regime [3,33,10] and the process to deduce the creep parameters is identical to that described earlier for the α phase. As shown in Figs. 9 and 10, the power-law exponent is 4.0 ± 0.6 while the activation energy is 220 kJ/mol, with a relatively large uncertainty of ± 60 kJ/mol owing to the limited data set. Therefore, the equation for power law creep in the β is

$$\dot{\gamma}_{p\beta} = 9 \times 10^{19} \frac{G}{T} \left(\frac{\bar{\tau}}{G} \right)^4 \exp \left(-\frac{220000}{RT} \right) /s \quad (17)$$

with the scaling parameter at the beginning of the equation varying between 1.7×10^{19} and $3 \times 10^{20}/s$.

There do not appear to be data for diffusional creep in the β region. Therefore, as a place-holder, we use the parameters assumed for the β -phase of zirconium in Sargent and Ashby [27]. Furthermore, although there are some data for creep in the mixed α and β region [Busby and White, 1979; Rosinger et al., 1979; [10]], they are so scarce to be of use in deducing the values of any parameters. Therefore, in this two-phase region, the creep rate is linearly interpolated between the models in the two single-phase regions.

2.1.5. Deformation mechanism map

The results of this section can be summarized in the form of a deformation mechanism map for unirradiated zircaloy-4 (Fig. 11). The map is drawn as contours of constant strain rate in a stress–temperature space. In general, all mechanisms are assumed to act simultaneously, and the boundaries between the different mechanisms are drawn when the dominant mechanisms switch. An exception to this is the transition to dislocation glide. For consistency between the strain rates in the different regimes a transition stress of $\bar{\tau}/G = 4.8 \times 10^{-3}$ had to be set below which dislocation glide is not active. This is equivalent to a narrow region in which the flow rate of the zircaloy is independent of temperature. While not particularly emphasized in the literature, close inspection of published deformation mechanism maps indicates that this is not an uncommon feature of many materials [9]. Furthermore, this regime has been specifically recognized in a number of experimental studies into the deformation of zircaloy-4 [5,14,32,17].

3. Implementation of multiple-mechanism model for creep into FEM

The constitutive equations described in the previous section have been incorporated into the ABAQUS[®] finite-element code, so that all possible mechanisms are evaluated at every location and time step. The actual creep rate at any point is determined by adding the rates from all the mechanisms that contribute simultaneously where physically appropriate, and by selecting the fastest of the mutually exclusive mechanisms. The advantage of this approach is that no *a priori* assumption about the creep law needs to be built into the FEM code. It is determined on the fly while the calculations proceed. This means that different portions of a structure can exhibit different creep mechanisms, depending on the

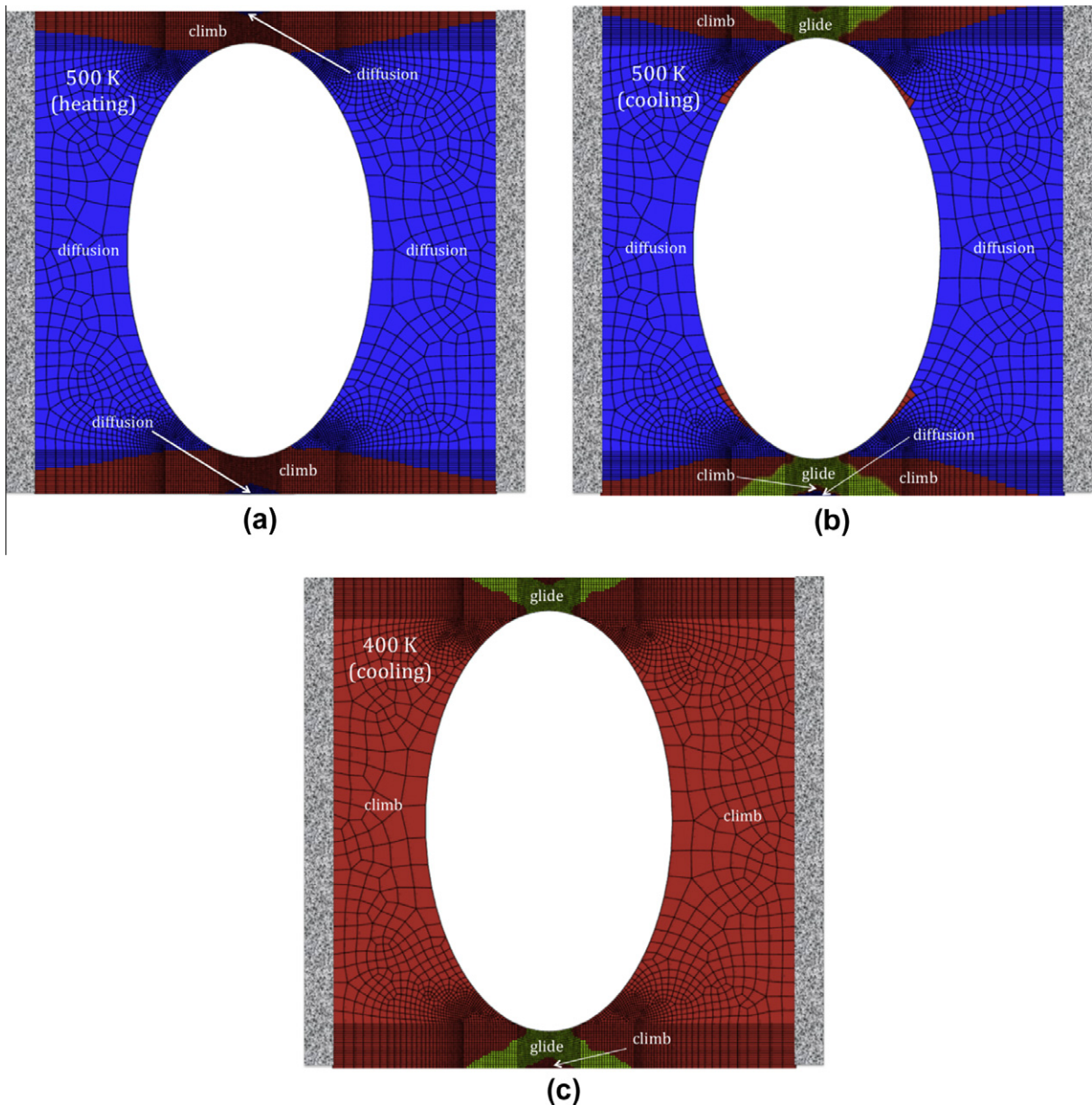


Fig. 13. The dominant relaxation mechanisms operating during thermal cycling of a clamped square sheet of zircaloy-4 containing an elliptical hole. The initial temperature was 400 K; the plate was heated at 0.01 K/s to 900 K, held for 6000 s then cooled at 0.1 K/s: (a) 500 K during the initial heating cycle; (b) 400 K during the cooling cycle; (c) 500 K during the cooling cycle.

local stress and temperature. Furthermore the same portion of a structure can exhibit different mechanisms with time, as either the stress or the temperature evolve. Both of these effects are illustrated by some model examples shown in the following section.

3.1. Numerical examples of zircaloy-4 plate with a hole

The first two examples are FEM calculations using the creep model described above for a sheet of zircaloy-4 (grain size of 75 μm) with a hole in it to generate a stress concentration. Fig. 12 shows the deformation mechanisms operating at 600 K after one second when a constant strain rate of 2.5×10^{-3} is applied to the ends of the sheet. A second example (Fig. 13) shows the same plate clamped at two ends at 400 K and then heated at a constant rate of 0.01 K/s to 900 K during a time period of 5×10^4 s. For these calculations, the coefficient of thermal expansion for zircaloy-4 was assumed to be $6 \times 10^{-6}/\text{K}$, [1], Poisson's

ratio was taken to be 0.342 [28], and the temperature-dependent shear modulus of Eq. (9) was used [28]. As in the similar problem considered by Thouless et al. [29], the stress level depends on the competition between the elastic stresses introduced by constrained thermal expansion and relaxation by creep. At low temperatures, the stresses build up elastically since the diffusional creep causes only limited relaxation. At higher temperatures and stresses, dislocation-climb mechanisms become dominant, starting in the high-stress region at the tip of the hole (Fig. 13a) and eventually spreading across the specimen. When the temperature is held at 900 K for 10^4 s there is extensive stress relaxation and the stresses fall to a level at which the dominant mechanism switches to diffusional creep. The cooling cycle at 0.1 K/s (Fig. 13b and c) induces tensile stresses that are relaxed rapidly at high temperatures, but build up at lower temperatures. Dislocation climb dominates for much of the cooling cycle, with glide becoming dominant at the stress concentrations, and eventually

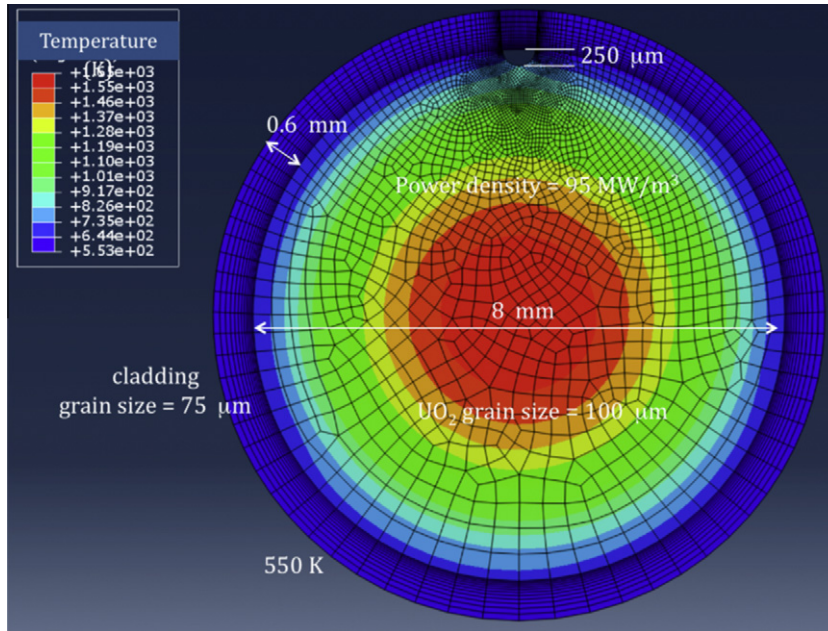


Fig. 14. Steady-state temperature profile for a cladding and fuel pellet with a power density of 95 MW/m³ and a surface temperature of 550 K.

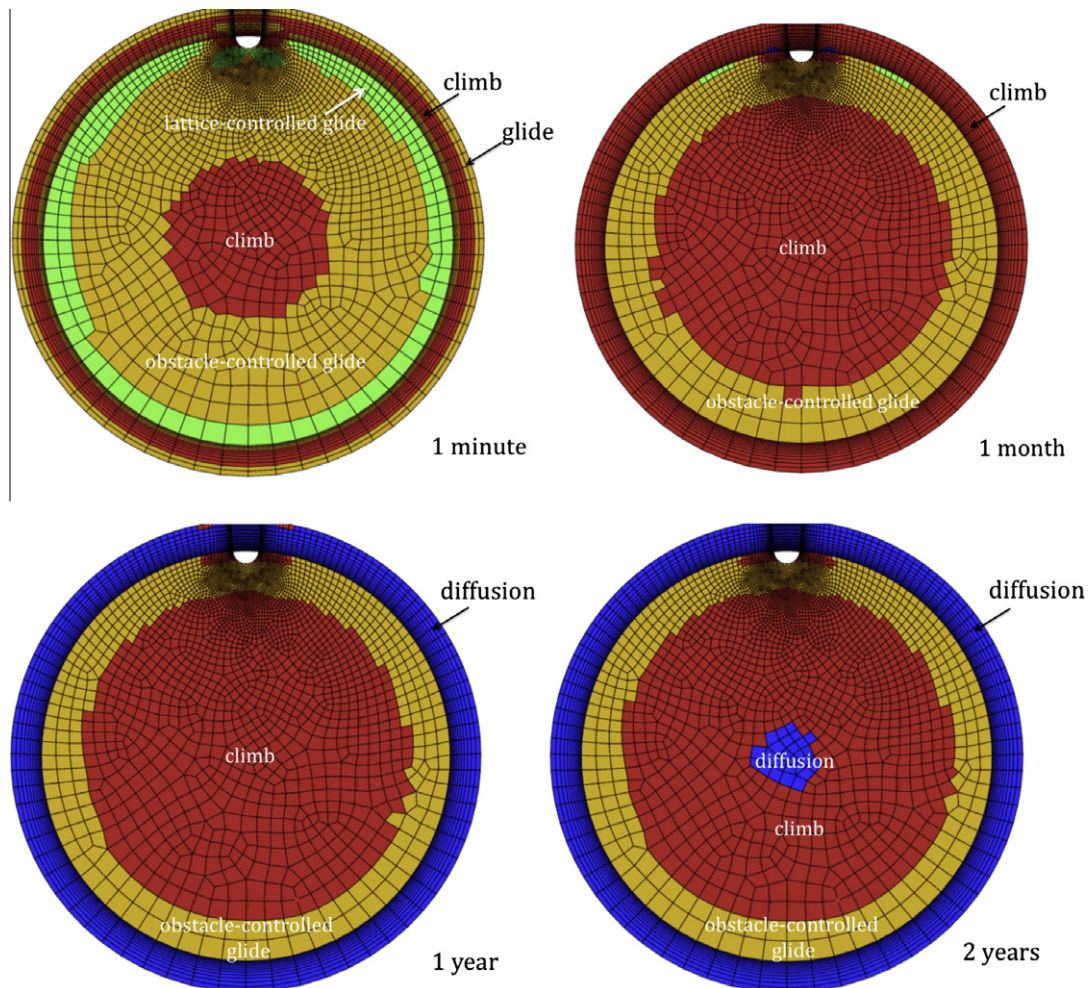


Fig. 15. Evolution of deformation mechanisms with time for the cladding and fuel assembly shown in Fig. 14.

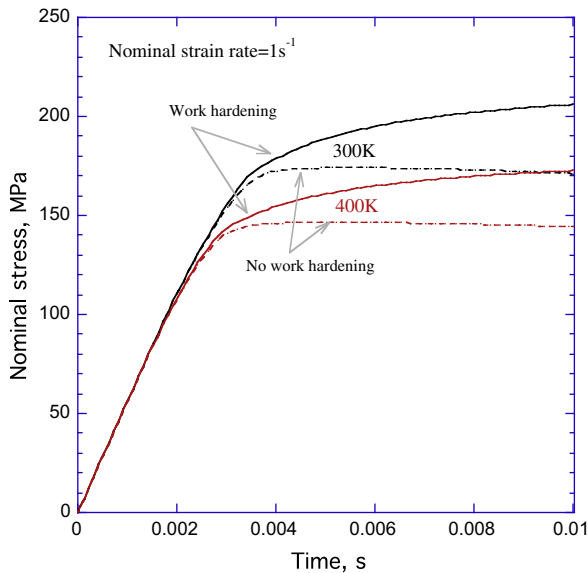


Fig. 16. Nominal stress–strain curves for the geometry of Fig. 12 with a nominal applied strain rate of 1/s, showing the effects of work hardening on the creep curves.

spreading across the specimen when the temperature is low enough. When the temperature is held at a low value, so that thermal contraction ceases, stress relaxation occurs with transitions from glide to diffusion mechanisms.

3.2. Numerical examples of zircaloy-4 as a cladding around a fuel rod

To provide an example of an analysis applicable to a fuel rod, we have analyzed the creep relaxation of a tube of zircaloy-4 (of thickness 600 μm) bonded to a cylinder of UO_2 fuel (of diameter 8.0 mm) with a semicircular chip in it (of depth 250 μm) as shown in Fig. 14. The equations for the creep mechanisms of UO_2 have been taken directly from Frost and Ashby [9], and have been incorporated into the finite-element code. Therefore, the model includes mechanistic creep models for both the cladding and the fuel. The specific heat capacity and thermal conductivity of zircaloy-4 were assumed to be 285 J/kg K and 21.5 W/m K [1]; the same elastic properties were used as in the previous examples. The specific heat capacity, thermal conductivity and coefficient of thermal expansion of UO_2 were assumed to be 236 J/kg K, 3.85 W/m K and $1.0 \times 10^{-5}/\text{K}$ [23]. The Young's modulus and Poisson's ratio of UO_2 were assumed to be 226 GPa and 0.315 [8]. The effects of radiation, such as swelling, growth and microstructural changes have not been included for either the fuel or cladding.

The calculations were performed by first computing the steady-state temperature profile shown in Fig. 14 assuming a power density of 95 MW/m^3 and a temperature of 550 K at the external surface of the cladding. This steady-state temperature profile was then imported into a 2-D plane-strain finite-element model to calculate the stresses and the creep rates using the multi-mechanism creep models for the zircaloy and the fuel. The evolution of the deformation mechanisms with time is shown in Fig. 15.

3.3. Effects of microstructure

The broad consistency of the creep data for the creep of zircaloy-4 in the literature suggests that the steady-state equations used in the numerical modeling are relatively robust and insensitive to details of the microstructure in the absence of radiation. However, ideally, a full multi-scale numerical model would be able

to integrate the effects of time, temperature, stress and radiation to calculate any microstructure-sensitive parameters, and then use these in the creep framework. Neither the models nor the experimental data in the literature are currently at a level where this might be possible. However, as discussed in Section 2.1.1, we do have an empirical relationship between τ_g and accumulated strain for use in the equation for dislocation glide; this can be assumed to represent the effect of an increased dislocation density on glide. Therefore, in this final set of calculations we demonstrate how it might be possible to construct a framework in which the creep parameters are updated in response to microstructural changes. This could be done by keeping track of the integrated strain, temperature, radiation and time for each element, and up-dating the creep parameters during each increment of calculation. Using this approach to analyze the geometry shown in Fig. 12, in which a strain is imposed on the edge of a plate with an elliptical hole in it, the effects of strain hardening can be seen in Fig. 16. In this figure, a comparison is made between the predictions that result when strain hardening is ignored and the predictions when strain hardening is included. The calculation uses Eq. (7) to compute the deformation associated with dislocation glide, so that the effects of temperature and time are accounted for, but also uses Eq. (6) to modify the creep parameter τ_g , for each element according to the total strain accumulated within it. However, an annealing model has not yet been built into the framework.

4. Conclusions

While deformation maps were first conceived and developed more than 30 years ago, there do not seem to have been significant attempts during the intervening period to incorporate the concepts of multi-mechanism models into a framework for continuum-level finite-element creep problems. However, the computing power now available makes this a relatively simple concept to implement. Such a framework allows the constitutive creep equations appropriate for a particular set of temperatures and stresses to be automatically invoked during a creep analysis, so that different mechanisms and creep equations can operate as appropriate in different regions and at different times during a finite-element analysis. From a creep-analysis perspective, this approach has many advantages: (i) the creep mechanism does not have to be postulated *a priori* before the analysis begins; (ii) design spaces can be extrapolated to regimes outside those covered by empirical equations; (iii) it lends itself to integration with lower-length scale models for microstructural changes; and (iv) different dominant mechanisms can be visualized as a function of space and time in the out-put of numerical calculations.

The mechanisms of creep for zircaloy-4 have been studied for many years. By re-analyzing the available experimental data, a deformation mechanism map has been developed for unirradiated zircaloy-4. This has then been used in illustrative examples of the multi-mechanism creep model. The consistency of all the experimental data for zircaloy-4 over four decades indicates that effects of microstructure and texture are reasonably small in the absence of radiation. This consistency means that useful analyses can be developed at the continuum level, and justifies the use of a continuum creep model that uses effective stresses for complex multi-axial stress states. However, there are clearly missing areas of experimental data that would be required for a more comprehensive model. In particular, the data for the diffusional creep that operates at low stresses are too limited to build an accurate model from.

To realize an ultimate goal of multi-scale modeling in a nuclear reactor, additional models need to be developed that would link the effects of radiation to creep, including radiation growth,

radiation creep, and changes in microstructure. While an on-going project will attempt to incorporate some of these effects into the creep frame-work, there are many aspects in which the present results should be of practical use. For example, in the problem of grid-to-rod fretting, different creep mechanisms play an important role in the deformation of the cladding, and in the relaxation of the contact stresses between the grid and the cladding (which will lead to fretting). Current empirical models apply only in a very limited temperature and stress range, which are not appropriate for all aspects of the problem. An accurate prediction of the changes in geometry and evolution of the contact stresses require an accurate creep model that can automatically capture the mechanism change, in addition to a detailed understanding of radiation effects. Furthermore, the development of continuum-level radiation creep models and correlation to experimental results will require these creep models, so that the effects of radiation and stress can be isolated from the effects of stress alone.

Acknowledgements

This research was supported by the Consortium for Advanced Simulation of Light Water Reactors (<http://www.casl.gov>), an Energy Innovation Hub (<http://www.energy.gov/hubs>) for Modeling and Simulation of Nuclear Reactors under U.S. Department of Energy Contract No. DE-AC05-00OR22725.

References

- [1] Allegheny Technologies, Reactor Grade Zirconium Alloys for Nuclear Waste Disposal. <<http://www.atimetals.com/businesses/business-units/wahchang/products/Documents/Zr%20nuke%20waste%20disposal.pdf>> (accessed 19.04.12).
- [2] I.M. Bernstein, *Trans. Metall. Soc. AIME* 239 (1967) 1518–1522.
- [3] C.C. Busby, L.S. White, Some High Temperature Mechanical Properties of Internally Pressurized Zircaloy-4 Tubing, WAPD-TM-1243, Westinghouse Electric Corporation, Pittsburgh, PA, 1976.
- [4] R.L. Coble, *J. Appl. Phys.* 34 (1963) 1679–1682.
- [5] J.L. Derep, S. Ibrahim, R. Rouby, G. Fantozzi, *Acta Metall.* 28 (1980) 607–619.
- [6] A.T. Donaldson, R.C. Ecob, *Scr. Metall.* 19 (1985) 1313–1318.
- [7] J. Fiala, J. Cadek, *Mater. Sci. Eng.* 75 (1985) 117–126.
- [8] J.K. Fink, M.G. Chasanov, L. Leibowitz, *J. Nucl. Mater.* 102 (1981) 17–25.
- [9] H.J. Frost, M.F. Ashby, *Deformation Mechanism Maps: The Plasticity and Creep of Metals and Ceramics*, Pergamon Press, Oxford, UK, 1982.
- [10] A.M. Garde, H.M. Chung, T.F. Kassner, *Acta Metall.* 26 (1997) 153–166.
- [11] T.A. Hayes, M.E. Kassner, R.S. Rosen, *Metall. Mater. Trans. A, Phys. Metall. Mater. Sci.* 33 (2002) 337–343.
- [12] T.A. Hayes, M.E. Kassner, *Metall. Mater. Trans. A* 37 (2006) 2389–2396.
- [13] C. Herring, *J. Appl. Phys.* 21 (1950) 437–445.
- [14] S.I. Hong, W.S. Ryu, C.S. Rim, *J. Nucl. Mater.* 116 (1983) 314–316.
- [15] D. Kaddour, S. Frechin, A.F. Gourgues, J.C. Brachet, L. Portier, A. Pineau, *Scr. Mater.* 51 (2004) 515–519.
- [16] D.B. Knorr, M.R. Notis, *J. Nucl. Mater.* 56 (1975) 18–24.
- [17] K.W. Lee, S.K. Kim, K.T. Kim, S.I. Hong, *J. Nucl. Mater.* 295 (2001) 21–26.
- [18] S.Y. Lee, K.T. Kim, S.I. Hong, *J. Nucl. Mater.* 392 (2009) 63–69.
- [19] Y. Matsuo, *J. Nucl. Sci. Technol.* 24 (1987) 111–119.
- [20] M. Mayuzumi, T. Onchi, *J. Nucl. Mater.* 175 (1990) 135–142.
- [21] F.R.N. Nabarro, *Bristol Conference on Strength of Solids* (1948) 75–90.
- [22] J. Novotny, J. Fiala, J. Cadek, *Acta Metall.* 33 (1985) 905–911.
- [23] S.G. Popov, V.K. Ivanov, J.J. Carbajo, G.L. Yoder, *Thermophysical Properties of MOX and UO₂ Fuels Including the Effects of Irradiation*, Oak Ridge National Laboratory, ORNL-TM-2000-35, 2000.
- [24] F. Povo, A.J. Marzocca, *J. Nucl. Mater.* 97 (1981) 323–332.
- [25] N. Prasad, G. Malakondaiah, P.R. Rao, *Scr. Metall.* 26 (1992) 541–543.
- [26] R. Raj, M.F. Ashby, *Metall. Trans.* 2 (1971) 1113–1127.
- [27] P.M. Sargent, M.F. Ashby, *Scr. Metall.* 16 (1982) 1415–1422.
- [28] M.L. Saux, J. Besson, S. Carassou, C. Poussard, X. Averty, *J. Nucl. Mater.* 378 (2008) 60–69.
- [29] M.D. Thouless, J. Gupta, J.M.E. Harper, *J. Mater. Res.* 8 (1993) 1845–1852.
- [30] B.V. Tanikella, K.L. Murty, *Transitions in biaxial creep of zircaloy-4 tubing*, in: Paper Presented at the 2nd Asia-Pacific Symp. Advances in Engineering Plasticity and its Application (AEP-2), Beijing, 1994.
- [31] Y. Wang, *Mechanical Anisotropy of Zircaloy-4: Temperature and Strain Rate Effects*, Ph.D Thesis, North Carolina State University, 1998.
- [32] J.-K. Yi, H.-B. Park, G.-S. Park, B.-W. Lee, *J. Nucl. Mater.* 189 (1992) 353–361.
- [33] H.E. Rosinger, P.C. Bera, W.R. Clendening, *J. Nucl. Mater.* 82 (1979) 286–297.